

Article

# Change-Point Detection in Functional First-Order Auto-Regressive Models

Algimantas Birbilas <sup>\*,†</sup>  and Alfredas Račkauskas <sup>\*,†</sup> 

Institute of Applied Mathematics, Vilnius University, Naugarduko g. 24, LT-03225 Vilnius, Lithuania

\* Correspondence: algimantas.birbilas@mif.vu.lt (A.B.); alfredas.rackauskas@mif.vu.lt (A.R.)

† These authors contributed equally to this work.

**Abstract:** A sample of continuous random functions with auto-regressive structures and possible change-point of the means are considered. We present test statistics for the change-point based on a functional of partial sums. To study their asymptotic behavior, we prove functional limit theorems for polygonal line processes in the space of continuous functions. For some situations, we use a block bootstrap procedure to construct the critical region and provide applications. We also study the finite sample behavior via simulations. Eventually, we apply the statistics to a telecommunications data sample.

**Keywords:** mean change-point detection; functional central limit theorem; functional sample; partial sums

**MSC:** 62R10

## 1. Introduction

A change-point in a sample is present when at least one statistical parameter changes, which may be caused by a variation in the mean, trend, or other parameters. Change-point detection has a broad range of applications, including financial time series analyses [1,2], econometrics [3], and climate change [4], to name a few. Given a sample of functional observations  $x_1(t), \dots, x_n(t)$ ,  $t \in [0, 1]$ , our goal is to detect the existence of a change-point such that before the change-point, samples are generated by a stationary functional auto-regressive process of the first-order, while after the change-point, stationarity is destroyed by the variation in the mean.

Statistical methods for functional observations were pioneered by Ramsey [5] in 1982. As the amount of high-resolution data has increased dramatically over the years, interest in functional data analysis (FDA) has emerged. In recent decades, multiple authors have contributed to the improvement of the theoretical FDA background—Kokoszka and Reimherr [6] and Ramsey et al. [7], to name few—and the practical implementation background of FDA in various fields—Ramsey et al. [8], Aneiros et al. [9], Alaya et al. [10], and Koerner et al. [11].

The first contribution to structural breaks in functional data was made by Berkes et al. [12], where a cumulative sum (CUSUM) test was proposed for independent functional data by using projections of the sample onto some principal components of covariance. Aue et al. [13] analyzed the limit distribution of a change-point estimator in the same setting. Horváth et al. [14] constructed a test for the stability of the autoregressive operator in a Hilbert-space-valued autoregressive process. Tests that do not rely on dimension reduction were derived by Horváth et al. [14] for general testing of stationarity and by Aue et al. [13] for functional break detection of  $m$ -dependent innovations. Structural break detection in the context of functional linear models was studied by Horváth and Reeder [15] and Aue et al. [13]. Smooth deviations from stationarity of functional time series in the frequency domain were



**Citation:** Birbilas, A.; Račkauskas, A. Change-Point Detection in Functional First-Order Auto-Regressive Models. *Mathematics* **2024**, *12*, 1889. <https://doi.org/10.3390/math12121889>

Received: 30 May 2024

Revised: 11 June 2024

Accepted: 14 June 2024

Published: 18 June 2024



**Copyright:** © 2024 by the authors. Licensee MDPI, Basel, Switzerland. This article is an open access article distributed under the terms and conditions of the Creative Commons Attribution (CC BY) license (<https://creativecommons.org/licenses/by/4.0/>).

investigated by Aue and van Delft [16]. Danielius and Račkauskas [17] suggested tests based on  $p$ -variation of functional CUSUM processes.

Still, a limited number of papers use functional approaches for telecommunications data. Aspirot et al. [18] studied a non-parametric regression model with the explanatory variable as a non-stationary dependent functional and the response variable as a scalar. Yu and Lambert [19] analyzed records for completed international calls. Birbilas and Račkauskas [20] modeled call data records and predicted mobile product consumption using different approaches in a functional framework. Change-point detection plays a crucial role in telecommunications as it can be monitored and implemented at different levels depending on the business model, e.g., the operational level (system failures in cell towers), the technical level (signal changes and wireless connection stability), and the marketing level (a promotion's effect on usage). Eventually, it has a significant effect at the business level, as accurate and timely detection of change-points is imperative for network operators to proactively address issues, optimize resource allocation, and ensure seamless service delivery. In other words, a change-point might identify improvement or, worse, system failure. System failures usually cost more than improvements. As telecommunications systems continue to evolve in complexity and scale, the application of sophisticated change-point detection techniques becomes increasingly indispensable for maintaining the integrity and functionality of this critical communication infrastructure.

Change-points are a relevant topic in both the scientific and telecommunications fields. In Shields et al. [21], the authors analyze collective behavior within smart cities using time-series-type call data record (CDR) data. The authors identify multiple change-points using three methods: binary segmentation, segmentation neighborhoods, and pruned extract linear time (PELT). They suggest that deviation from normal collective mobility patterns can be explained by known significant events in the city. Loreh John [22] provides a study using change-point analysis to detect changes in the mean for the wireless telecommunications field. The author uses a previously known likelihood method and suggests a new maximum distance of the running means method to identify locations of the change-points within the 2G network. One of the latest works in this area is by Aleksiejunas and Garuolis [23] and is devoted to traffic change-points; it utilizes machine learning methods such as long short-term memory (LSTM) and recurrent neural networks (RNNs). The authors apply change-point identification algorithms for synthetic data and reuse algorithms for the spatial traffic distributions of LTE (Long Term Evolution) mobile networks.

Recall that for a separable Banach space  $B$  with a norm  $\|x\|_B, x \in B, C[0, 1], B$  is a separable Banach space of continuous functions  $f : [0, 1] \rightarrow B$  endowed with the norm  $\|f\|_{B, \infty} = \max_{0 \leq t \leq 1} \|x(t)\|_B, f \in C([0, 1], B)$ . We abbreviate  $C([0, 1], R)$  as  $C[0, 1]$  and  $\|x\|_{R, \infty}$  as  $\|x\|_{\infty}$ . For a given random sample  $X_1(t), \dots, X_n(t), t \in [0, 1]$ , with values in the space  $C[0, 1]$ , we consider the following model:

$$X_k - \mu = \beta(X_{k-1} - \mu) + g(k/n) + Y_k, \quad (1)$$

where  $\beta : C[0, 1] \rightarrow C[0, 1]$  is a linear bounded operator,  $\mu \in C[0, 1]$ , the function  $g : [0, 1] \rightarrow C[0, 1]$  is deterministic, and  $Y_i = (Y_i(t), t \in [0, 1]), i \in \mathbb{Z}$ , is a sequence of independent and identically distributed (iid) random variables with values in the space  $C[0, 1]$  and defined on a complete probability space  $(\Omega, \mathcal{F}, P)$ .

We analyze this model while keeping in mind the telecommunications data coming from call data records (CDRs). This data set contains the usage of three mobile products: voice calls, SMS, and mobile data. For the case study, voice consumption in minutes and mobile data consumption in MB are used. This type of data was analyzed in [20] using first-order auto-regressive models, and it was confirmed that models of type (1) are appropriate.

Throughout,  $Y = (Y(t), t \in [0, 1])$  denotes a generic element of the sequence  $(Y_i, i \in \mathbb{Z})$  for which the following assumption shall be used.

**Assumption 1** (Assumption (A)).  $Y$  is a mean-zero  $C[0, 1]$ -random variable with covariance function  $q$ ,  $q(t, s) = EY(t)Y(s)$ ,  $t, s \in [0, 1]$ , and satisfies the central limit theorem (denoted  $Y \in CLT(C[0, 1])$ ).

Recall that  $Y \in CLT(C[0, 1])$  means that there exists a mean-zero Gaussian random variable (denoted  $\mathcal{N}_q$ ) in  $C[0, 1]$  with covariance  $q$  such that the sequence  $(n^{-1/2}(Y_1 + \dots + Y_n), n \geq 1)$  converges in a distribution to  $\mathcal{N}_q$ . It is well known that if there exists a random variable  $M$  such that  $EM^2 < \infty$  and

$$|Y(t) - Y(s)| \leq M|t - s|^\alpha, \quad s, t \in [0, 1],$$

with some  $\alpha \in (0, 1]$ , then  $Y \in CLT(C[0, 1])$ .

Throughout, we assume

$$\|\beta\| := \sup_{\|x\|_\infty < 1} \|\beta(x)\|_\infty < 1. \tag{2}$$

This assumption guaranties that the inverse operator  $(I - \beta)^{-1}$  exists, where  $I$  is the identity operator, and has the expansion

$$(I - \beta)^{-1} = \sum_{k=0}^{\infty} \beta^k.$$

Our main aim is to test the hypothesis

$$H_0 : g = 0 \text{ versus } H_1 : g \neq 0, \tag{3}$$

with emphasis on the case of change-point detection, which corresponds to a piecewise constant function  $g$  with respect to the first argument.

The model under consideration covers both abrupt as well continuous variations of a sample mean. Test statistics and their asymptotic distributions under the null hypothesis as well under various alternatives are established and presented in Section 2. Section 3 contains a description of the testing procedure. The main challenge here is to find critical levels. The solution for this problem is proposed via the Monte Carlo method. Section 4 contains a simulation study. Finally, Section 5 deals with a concrete data set related to telecommunication problems.

### 2. Auxiliary Results

For each  $n \geq 1$ , consider the random sample  $Z_0, Z_1, \dots, Z_n$  in  $C[0, 1]$  satisfying

$$Z_0 = 0, \quad Z_i = \beta Z_{i-1} + f(i/n)r_n + Y_i, \quad i = 1, \dots, n,$$

where  $r_n \in C[0, 1]$ , and  $f : [0, 1] \rightarrow \mathbb{R}$ . Consider a polygonal line process  $\zeta_n = (\zeta_n(t), t \in [0, 1])$  defined by

$$\zeta_n(t) = \sum_{k=1}^{\lfloor nt \rfloor} Z_k + (nt - \lfloor nt \rfloor)Z_{\lfloor nt \rfloor + 1} = \sum_{k=1}^n Z_k e_{nk}(t), \tag{4}$$

where

$$e_{nk}(t) = \begin{cases} 0 & \text{if } t < (k-1)/n, \\ tn - (k-1) & \text{if } (k-1)/n \leq t \leq k/n, \\ 1 & \text{if } t > k/n. \end{cases}$$

Let  $W_q = (W_q(t), t \in [0, 1])$ , be a  $C[0, 1]$ -valued Wiener process corresponding to covariance  $q$  in such a way that  $W_q$  is a  $C[0, 1]$ -valued mean-zero Gaussian process with independent increments such that  $W_q(s) - W_q(t)$  has the same distribution as  $\mathcal{N}_q|t - s|^{1/2}$ .

Recall, that for a function  $f : [0, 1] \rightarrow R$ ,

$$v_1(f, [a, b]) := \sup \left\{ \sum_{k=1}^m |f(\tau_k) - f(\tau_{k-1})| : a = \tau_0 < \tau_1 < \dots < \tau_{m-1} < \tau_m = b, m \geq 1 \right\}.$$

The function  $f$  has finite variation if  $v_1(f) := v_1(f : [0, 1]) < \infty$ .

**Lemma 1.** Assume that  $Y$  satisfies Assumption 1, and

(a) There is a continuous function  $r : [0, 1] \rightarrow R$  such that

$$\lim_{n \rightarrow \infty} \|\sqrt{nr_n} - r\|_\infty = 0; \tag{5}$$

(b) The function  $f : [0, 1] \rightarrow R$  is bounded and has finite variation.

Then

$$n^{-1/2}(I - \beta)\zeta_n \xrightarrow{\mathcal{D}} W_q + h_{r,f} \text{ in the space } C([0, 1], C[0, 1]),$$

where

$$h_{r,f}(t) = \int_0^t f(s)dsr, \quad t \in [0, 1].$$

**Proof of Lemma 1.** Consider a linear process  $(\tilde{Z}_k, k \geq 1)$  with values in  $C[0, 1]$  defined by

$$\tilde{Z}_k = \sum_{j=0}^\infty \beta^j Y_{k-j} = \sum_{j=-\infty}^k \beta^{k-j} Y_j, \quad k = 0, 1, 2, \dots$$

Note that the series above converge a.s. in  $C[0, 1]$  so that  $\tilde{Z}_k$  is correctly defined and is a  $C[0, 1]$ -valued random variable for each  $k \geq 0$ . Indeed,

$$E \left\| \sum_{j=m}^n \beta^j Y_{k-j} \right\| \leq \sum_{j=m}^n \|\beta\|^j E\|Y\| \rightarrow 0 \text{ as } m, n \rightarrow \infty$$

yields convergence in the probability of the series  $\sum_j \beta^j Y_{k-j}$ . As  $(Y_i)$  are independent, the Ito–Nisio theorem ensures a.s.-convergence as well. Next, we consider a  $C[0, 1]$ -valued polygonal line process  $\tilde{\zeta}_n$  defined by

$$\tilde{\zeta}_n(t) = \sum_{k=1}^{\lfloor nt \rfloor} \tilde{Z}_k + (nt - \lfloor nt \rfloor) \tilde{Z}_{\lfloor nt \rfloor + 1} = \sum_{k=1}^n \tilde{Z}_k e_{nk}(t), \quad t \in [0, 1]. \tag{6}$$

We have by [24] (see Theorem 5 therein)

$$n^{-1/2}(I - \beta)\tilde{\zeta}_n \xrightarrow{\mathcal{D}} W_q \text{ in the space } C([0, 1], C[0, 1]), \tag{7}$$

Since  $Z_k$  can be expressed by

$$Z_k = \sum_{j=1}^k \beta^{k-j} Y_j + \sum_{j=1}^k \beta^{k-j} f(j/n)r_n = \sum_{j=1}^k \beta^{k-j} Y_j + \sum_{j=0}^{k-1} \beta^j f((k-j)/n)r_n,$$

we have

$$Z_k - \tilde{Z}_k = \sum_{j=0}^{k-1} \beta^j f((k-j)/n)r_n - \sum_{j=-\infty}^0 \beta^{k-j} Y_j.$$

This yields

$$n^{-1/2}\zeta_n(t) = n^{-1/2}\hat{\zeta}_n(t) + \Delta_n(t), \quad t \in [0, 1], \tag{8}$$

where  $\Delta_n(t) = n^{-1/2}[\zeta_n(t) - \tilde{\zeta}_n(t)]$ . We claim that

$$\max_{0 \leq t \leq 1} \left\| \Delta_n(t) - (I - \beta)^{-1} r \int_0^t f(s) ds \right\|_{C[0,1]} \xrightarrow[n \rightarrow \infty]{P} 0. \tag{9}$$

To prove this claim, first we decompose

$$\Delta_n(t) = \Delta'_n(t) + \Delta''_n(t), \quad t \in [0, 1],$$

where

$$\Delta'_n(t) = n^{-1/2} \sum_{k=1}^n \left[ \sum_{j=0}^{k-1} \beta^j f((k-j)/n) r_n \right] e_{nk}(t), \quad \Delta''_n(t) = n^{-1/2} \sum_{k=1}^n \left[ \sum_{j=-\infty}^0 \beta^{k-j} Y_j \right] e_{nk}(t).$$

Since  $\Delta''(t) = n^{-1/2} \tilde{Z}_0 \sum_{k=1}^n \beta^k e_{nk}(t)$ , we see that  $\max_{0 \leq t \leq 1} \|\Delta''_n\|_{C[0,1]} \xrightarrow[n \rightarrow \infty]{P} 0$ , and (9) reduces to

$$\max_{0 \leq t \leq 1} \left\| \Delta'_n(t) - (I - \beta)^{-1} r \int_0^t f(s) ds \right\|_{C[0,1]} \xrightarrow[n \rightarrow \infty]{P} 0. \tag{10}$$

Write  $n^{-1/2} \Delta'_n(t) = \Delta_{n1}(t) + \Delta_{n2}(t)$ , where

$$\Delta_{n1}(t) = n^{-1} \sum_{k=1}^n \left[ \sum_{j=0}^{k-1} \beta^j f((k-j)/n) r \right] e_{nk}(t)$$

and

$$\Delta_{n2}(t) = n^{-1} \sum_{k=1}^n \left[ \sum_{j=0}^{k-1} \beta^j f((k-j)/n) (\sqrt{nr} r_n - r) \right] e_{nk}(t).$$

Next, observe that

$$\|\Delta_{n2}(t)\|_{C[0,1]} \leq \|f\|_{\infty} (1 - \|\beta\|)^{-1} \|\sqrt{nr} r_n - r\|_{C[0,1]},$$

since  $\sum_{k=1}^n e_{nk}(t) = nt$ . By condition (5),  $\lim_{n \rightarrow \infty} \max_{0 \leq t \leq 1} \|\Delta_{n2}(t)\|_{C[0,1]} = 0$  and (10) reduces to

$$\max_{0 \leq t \leq 1} \left\| \Delta_{n1}(t) - (I - \beta)^{-1} r \int_0^t f(s) ds \right\|_{C[0,1]} \rightarrow 0. \tag{11}$$

Consider the functions

$$I_n(h, t) = n^{-1} \sum_{k=1}^n f(k/n - h) e_{nk}(t), \quad I(h, t) = \int_0^t f(s - h) ds,$$

We have

$$\begin{aligned} |I_n(h, t) - I(h, t)| &= \left| \sum_{k=1}^n \int_{(k-1)/n}^{k/n} [f(k/n - h) - f(s - h)] \mathbf{1}_{[0,t]}(s) ds \right| \\ &\leq \sum_{k=1}^n \int_{(k-1)/n}^{k/n} |f(k/n - h) - f(s - h)| ds \\ &\leq n^{-1} \sum_{k=1}^n v(f(\cdot - h) : [(k-1)/n, k/n]) \leq n^{-1} v(f : [-h, 1 - h]) \\ &\leq n^{-1} v(f : [0, 1]) \end{aligned}$$

Next, we observe that

$$|I(h, t) - I(0, t)| \leq \int_0^t |f(s - h) - f(s)| ds \rightarrow 0 \text{ as } h \rightarrow 0.$$

Fix  $J \geq 1$ . Then for each  $\varepsilon > 0$ , we find  $N_\varepsilon \geq 1$  such that

$$|I(j/n, t) - I(0, t)| \leq \int_0^t |f(s - h) - f(s)| ds < \varepsilon \text{ if } n \geq N_\varepsilon, j \leq J.$$

Since  $f(t) = 0$  for  $t \leq 0$ ,

$$\begin{aligned} \Delta_{n1}(t) &= n^{-1} \sum_{k=1}^n \sum_{j=0}^k \beta^j r f((k-j)/n) e_{nk}(t) \\ &= \sum_{k=1}^n \sum_{j=0}^n \beta^j r f((k-j)/n) e_{nk}(t) = \sum_{j=0}^n \beta^j r \sum_{k=1}^n f((k-j)/n) e_{nk}(t) \\ &= \sum_{j=0}^\infty \beta^j r I_n(j/n, t). \end{aligned}$$

This yields

$$\begin{aligned} \max_{0 \leq t \leq 1} \left\| \Delta_{n1}(t) - (I - \beta)^{-1} r \int_0^t f(s) ds \right\|_{C[0,1]} &= \left\| \sum_{j=0}^\infty \beta^j r I_n(j/n, t) - \sum_{j=0}^\infty \beta^j r I(0, t) \right\|_{C[0,1]} \\ &\leq \sum_{j=0}^J \|\beta^j\| r \varepsilon + 2\|f\|_\infty \sum_{j=J}^\infty \|\beta\|^j \|r\| \end{aligned}$$

Letting  $J \rightarrow \infty$  gives

$$\max_{0 \leq t \leq 1} \left\| \Delta_{n1}(t) - (I - \beta)^{-1} r \int_0^t f(s) ds \right\|_{C[0,1]} \leq \frac{\|r\|}{1 - \|\beta\|} \varepsilon.$$

Since  $\varepsilon > 0$  is arbitrary, this yields (11) and completes the proof.  $\square$

Consider an operator  $L : C([0, 1], C[0, 1]) \rightarrow C([0, 1], C[0, 1])$  defined by  $Lx(t) = x(t) - tx(1), t \in [0, 1], x \in C([0, 1], C[0, 1])$ . Define a  $C[0, 1]$ -valued Brownian bridge  $B_q = (B_q(t), t \in [0, 1])$ , by

$$B_q(t) = W_q(t) - tW_q(1) = LW_q(t).$$

**Lemma 2.** Under the conditions of Lemma 1,

$$n^{-1/2}(I - \beta)L\zeta_n \xrightarrow{\mathcal{D}} B_q + Lh_{r,f} \text{ in the space } C([0, 1], C[0, 1]),$$

where

$$Lh_{r,f}(t) = h_{r,f}(t) - th_f(1) = \left[ \int_0^t f(s) ds - t \int_0^1 f(s) ds \right] r, t \in [0, 1].$$

**Proof of Lemma 2.** Since  $L$  is a continuous operator, the result follows from Lemma 1 and the continuous mapping theorem (Billingsley [25] Theorem 2.7).  $\square$

### 3. Test Statistics and Their Asymptoticity

Define

$$M_{n,\beta} := \max_{1 \leq k \leq n} \max_{0 \leq t \leq 1} \left| (I - \beta) \sum_{j=1}^k X_j(t) \right|, \tag{12}$$

and

$$T_{n,\beta} = \max_{1 \leq k \leq n} \max_{0 \leq t \leq 1} \left| (I - \beta) \sum_{j=1}^k (X_j(t) - \bar{X}_n(t)) \right|, \tag{13}$$

where  $\bar{X}_n = n^{-1}(X_1 + \dots + X_n)$ . Statistic  $M_{n,\beta}$  is adopted for testing (3) if  $\mu = 0$ , whereas  $T_{n,\beta}$  can be used for testing (3) in the case where we have  $\mu \neq 0$ .

**Theorem 1.** For the model (1), assume that  $Y$  satisfies Assumption 1 and  $\mu = 0, g = 0$ . Then

$$n^{-1/2}M_{n,\beta} \xrightarrow{\mathcal{D}} M_q := \max_{0 \leq t \leq 1} \|W_q(t)\|_{C[0,1]}. \tag{14}$$

**Proof of Theorem 1.** By Lemma 1 and the continuous mapping theorem,

$$n^{-1/2}\|(I - \beta)\zeta_n\|_{C[0,1],\infty} \xrightarrow{\mathcal{D}} \|W_q\|_{C[0,1],\infty}. \tag{15}$$

Observing that  $M_{n,\beta} = \|(I - \beta)\zeta_n\|_{C[0,1],\infty}$  and  $M_q = \|W_q\|_{C[0,1],\infty}$  completes the proof.  $\square$

**Theorem 2.** For the model (1), assume that  $Y$  satisfies Assumption 1 and  $g = 0$ . Then

$$n^{-1/2}T_{n,\beta} \xrightarrow{\mathcal{D}} T_q := \max_{0 \leq t \leq 1} \|B_q(t)\|_{C[0,1]}. \tag{16}$$

**Proof of Theorem 2.** Since substituting  $X_k$  with  $X_k - \mu$  does not change the statistic  $T_{n,\beta}$ , we assume  $\mu = 0$ . The function  $L : C([0, 1], C[0, 1])$  is continuous; hence, by the continuous mapping theorem,  $n^{-1/2}L\zeta_n \xrightarrow{\mathcal{D}} LW_q$ . Applying the continuous mapping theorem once more yields

$$n^{-1/2} \max_{0 \leq t \leq n} \|(I - \beta)L\zeta_n(t)\|_{C[0,1]} \xrightarrow{\mathcal{D}} \max_{0 \leq t \leq 1} \|LW_q(t)\|_{C[0,1]}.$$

Next, we notice that  $\max_{0 \leq t \leq n} \|(I - \beta)L\zeta_n(t)\|_{C[0,1]} = T_{n,\beta}$ , whereas  $LW_q = B_q$ . This completes the proof.  $\square$

**Theorem 3.** Assume for the model (1) that  $Y$  satisfies Assumption 1,  $g(s, t) = g_n(s, t) = f(s)r_n(t)$  satisfies  $\sqrt{nr_n} \rightarrow r$  in  $C[0, 1]$ , and the function  $f : [0, 1] \rightarrow R$  is bounded and has finite variation. Then

$$n^{-1/2}T_{n,\beta} \xrightarrow{\mathcal{D}} T_{q,r} := \max_{0 \leq t \leq 1} \left\| B_q(t) + \left[ \int_0^t f(s)ds - t \int_0^1 f(s)ds \right] r \right\|_{C[0,1]}, \tag{17}$$

Particularly, if  $\lim_{n \rightarrow \infty} \sqrt{n} \max_{0 \leq t \leq 1} |r_n(t)| = \infty$ , then

$$n^{-1/2}T_{n,\beta} \xrightarrow[n \rightarrow \infty]{P} \infty. \tag{18}$$

**Proof of Theorem 3.** The proof follows from Lemma 2 and the continuous mapping theorem.  $\square$

**Theorem 4.** Assume for model (1) that  $Y$  satisfies Assumption 1,  $g = 0$ , and  $\mu = \mu_n$  satisfies  $\sqrt{n}\mu_n \rightarrow r$  in  $C[0, 1]$ . Then

$$n^{-1/2}M_{n,\beta} \xrightarrow{\mathcal{D}} M_{q,r} := \max_{0 \leq t \leq 1} \|W_q(t) + r\|_{C[0,1]}. \tag{19}$$

Particularly, if  $\lim_{n \rightarrow \infty} \sqrt{n} \max_{0 \leq t \leq 1} |\mu_n(t)| = \infty$ , then

$$n^{-1/2}M_{n,\beta} \xrightarrow[n \rightarrow \infty]{P} \infty. \tag{20}$$

**Proof of Theorem 4.** The proof follows from Lemma 1 and the continuous mapping theorem.  $\square$

**Remark 1.** In practice, the auto-regression operator  $\beta$  is unknown and has to be substituted with its consistent estimator  $\hat{\beta}$ . This substitution can be controlled through the following convergence:

$$\left| n^{-1/2}M_{n,\beta} - n^{-1/2}M_{n,\hat{\beta}} \right| \leq \|\beta - \hat{\beta}\| \cdot \|(I - \beta)^{-1}\| n^{-1/2}M_{n,\beta} \xrightarrow[n \rightarrow \infty]{P} 0$$

provided  $\|\beta - \hat{\beta}\| \xrightarrow[n \rightarrow \infty]{P} 0$ .

The simulations below (Figures 16 and 17) confirm this remark.

#### 4. Testing Procedure

Assume that the functional sample  $X_1, \dots, X_n$  follows model (1). Consider the null hypothesis  $H_0 : g = 0$ . For a fixed  $0 \leq \alpha < 1$ , let  $C_\alpha$  and  $C'_\alpha$  be solutions of equations

$$P(M_q > C_\alpha) = \alpha \text{ and } P(T_q > C'_\alpha) = \alpha \tag{21}$$

respectively. According to Theorems 1 and 2, the tests

$$n^{-1/2}M_{n,\beta} > C_\alpha \text{ and } n^{-1/2}T_{n,\beta} > C'_\alpha \tag{22}$$

have an asymptotic significance level of  $\alpha$ .

If  $q$  is known, then by the Kuelbs [26] invariance principle, as  $N \rightarrow \infty$ ,

$$F_{q,N}(x) := P\left(N^{-1/2} \max_{1 \leq k \leq N} \max_{0 \leq s \leq 1} \left| \sum_{j=1}^k \xi_{qj}(s) \right| \leq x\right) \rightarrow P(M_q \leq x), \quad x \geq 0,$$

where  $\xi_{gj}, j = 1, \dots, N$  are iid Gaussian random variables in  $C[0, 1]$  with mean zero and covariance  $q$ . Hence, an approximate solution of the first equation in (21) can be found from

$$1 - F_{q,N}(C_\alpha) = \alpha \tag{23}$$

by the Monte Carlo method. Similarly, as  $N \rightarrow \infty$ ,

$$\tilde{F}_{q,N}(x) := P\left(N^{-1/2} \max_{1 \leq k \leq N} \max_{0 \leq s \leq 1} \left| \sum_{j=1}^k \xi_{qj}(s) - M^{-1} \sum_{j=1}^n \xi_{qj}(s) \right| \leq x\right) \rightarrow P(T_q \leq x), \quad x \geq 0,$$

and an approximate solution of the second equation in (21) can be found by the Monte Carlo method from

$$1 - \tilde{F}_{q,N}(C'_\alpha) = \alpha. \tag{24}$$

Particularly, if  $(Y_k, k \geq 1)$  are iid standard Wiener processes, then  $q(s, t) = \min\{s, t\}$ ,  $s, t \in [0, 1]$ , and again, denoting

$$F_{M,N}(x) = P\left(N^{-1/2}M^{-1/2} \max_{1 \leq k \leq N} \max_{1 \leq m \leq M} \left| \sum_{j=1}^k \sum_{i=1}^m \gamma_{ij} \right| \leq x\right),$$

where  $(\gamma_{ij}, i = 1, \dots, N, j = 1, \dots, M)$  are iid standard normal random variables, and using the Donsker invariance principle, the solution of (23) can be approximated by the solution of the following equation:

$$1 - F_{M,N}(C_\alpha) = \alpha. \tag{25}$$

Similarly, (24) can be approximated by

$$1 - \tilde{F}_{M,N}(C'_\alpha) = \alpha, \tag{26}$$

where

$$\tilde{F}_{M,N}(x) = P\left(N^{-1/2}M^{-1/2} \max_{1 \leq k \leq N} \max_{1 \leq m \leq M} \left| \sum_{j=1}^k \sum_{i=1}^m [\gamma_{ij} - M^{-1} \sum_{i=1}^M \gamma_{ij}] \right| \leq x\right), \quad x > 0.$$

Density functions of the distribution functions  $F_{N,M}$  and  $\tilde{F}_{M,N}$  (with  $M = N = 1000$ ) were generated using kernel (Epanechnikov) density estimates and  $MC \in \{100, 400, 500, 800, 1000\}$  replications of the corresponding random variables (see Figure 1). We see that the effect of the number of MC replications is minimal.

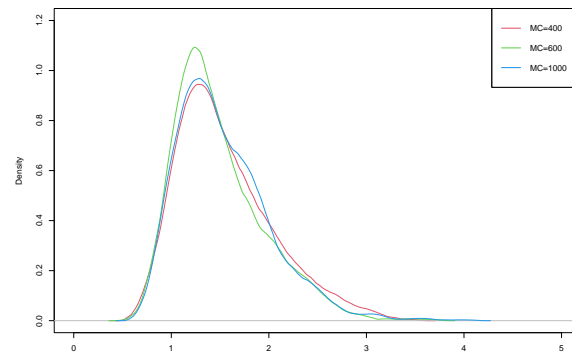


**Figure 1.** Kernel (Epanechnikov) density functions of  $F_{M,N}$  obtained with different numbers of Monte Carlo simulations:  $MC = (400, 600, 1000)$ , and  $N = 1000, M = 1000$ .

Equations (25) and (26) can be solved by the Monte Carlo method. The obtained quantile values of  $C_\alpha$  and  $C'_\alpha$  are presented in Tables 1 and 2.

**Table 1.**  $\alpha$  quantiles of  $F_{M,N}, M = N = 1000$ .

| $\alpha$  | 0.005  | 0.01   | 0.025  | 0.05   | 0.25   | 0.5    | 0.75   | 0.95   | 0.975  | 0.99   | 0.995  |
|-----------|--------|--------|--------|--------|--------|--------|--------|--------|--------|--------|--------|
| MC = 400  | 0.8082 | 0.8266 | 0.8606 | 0.8982 | 1.1622 | 1.4163 | 1.7689 | 2.5414 | 2.6921 | 2.9071 | 2.9927 |
| MC = 600  | 0.8062 | 0.8562 | 0.8965 | 0.9412 | 1.1957 | 1.4358 | 1.8070 | 2.5188 | 2.7242 | 3.2369 | 3.3202 |
| MC = 800  | 0.7636 | 0.8120 | 0.8779 | 0.9413 | 1.1853 | 1.4317 | 1.7576 | 2.4568 | 2.6881 | 2.9427 | 3.1688 |
| MC = 1000 | 0.7897 | 0.8176 | 0.8857 | 0.9322 | 1.1690 | 1.4240 | 1.7919 | 2.4478 | 2.7043 | 2.9565 | 3.1000 |

**Table 2.**  $\alpha$  quantiles of  $\tilde{F}_{M,N}, M = N = 1000$ .

| $\alpha$  | 0.005  | 0.01   | 0.025  | 0.05   | 0.25   | 0.5    | 0.75   | 0.95   | 0.975  | 0.99   | 0.995  |
|-----------|--------|--------|--------|--------|--------|--------|--------|--------|--------|--------|--------|
| MC = 400  | 0.7489 | 0.7682 | 0.7988 | 0.8313 | 1.0401 | 1.2276 | 1.4700 | 1.9317 | 2.0333 | 2.1389 | 2.2285 |
| MC = 600  | 0.7509 | 0.7809 | 0.8214 | 0.8649 | 1.0425 | 1.2301 | 1.4860 | 1.9290 | 2.1213 | 2.3126 | 2.6485 |
| MC = 800  | 0.7514 | 0.7745 | 0.8266 | 0.8751 | 1.0401 | 1.2257 | 1.4606 | 1.9188 | 2.0661 | 2.2002 | 2.4172 |
| MC = 1000 | 0.7313 | 0.7520 | 0.8111 | 0.8606 | 1.0397 | 1.2230 | 1.4336 | 1.8510 | 2.0777 | 2.2900 | 2.3669 |

The true critical value  $C_n(\alpha)$  for the test statistic  $M_{n,\beta}$  corresponding to the pre-designated significance level  $\alpha \in (0, 1)$  is defined as a solution of the following equation:

$$P(M_{n,\beta} > C_n(\alpha) | H_0) = \alpha \tag{27}$$

the exact solution of which can be obtained only in some very special cases. Therefore, critical values obtained from asymptotic distribution theory are widely used in applications. However, this usually requires a very large sample size since first-order asymptotic theory often gives poor approximations of the distributions of test statistics.

Another way to solve Equation (27) is the block bootstrap procedure, as it can assist us with the approximation of critical values. In the works of Härdle et al. [27], Kunsch [28], and Liu and Singh [29], we find multiple algorithms on how to construct the block bootstrap

for time series data. There exist numerous variants of the block bootstrap method that can mainly be distinguished by whether the blocks are overlapping or not and whether the block length is fixed or increasing. The overall block bootstrap idea, however, involves partitioning of the sample into sub-blocks and then independently drawing these sub-blocks until the sample size is attained. Adapted to our case, a block bootstrap method with fixed length  $l$  and overlapping blocks is performed based on the work of Nyarige [30]. We take the algorithm from Nyarige [30] and adapt it to the overlapping case: see Algorithm 1. The application of the procedure will be presented in the simulation study.

---

**Algorithm 1** Block bootstrap procedure

---

1. Given the sample  $\{ X_1, \dots, X_n \}$ , using a suitable rule, choose the fixed block length,  $l$ , and partition the sample into  $B$  overlapping blocks, each with the given length  $l$ . As blocks can overlap,  $B = n - l + 1$ .
  2. Draw randomly for a replacement from the resulting blocks and order the drawn blocks from end-to-end to form a new bootstrap sample  $\{ X_1^*, \dots, X_n^* \}$ .
  3. Compute the statistic of interest in the same way as for the original sample.
- 

We discuss asymptotic critical value adjustments afterwards. In the case where  $(Y_k)$  are iid standard Brownian motions and the operator  $\beta$  is multiplied by a function, we generate 500 Monte Carlo simulations  $M_{n,\beta}$  under  $H_0$  to have a test statistics sample  $\{M_{n,\beta}^1, \dots, M_{n,\beta}^{500}\}$ . Epanechnikov kernel density plots of the sample  $\{M_{n,\beta}^1, \dots, M_{n,\beta}^{500}\}$  and of  $M_q$  are shown in Figure 2. The Monte Carlo experiment provides evidence that the true and nominal probabilities that the test makes a Type I error can be notably dissimilar when an asymptotic critical value is used. Critical value adjustments can be made with the help of a Bonferroni correction: see Haynes [31] for more details and Sedgwick [32] for an application example. One can see that the Monte Carlo experiment density (blue density) is pushed to the left in comparison to the asymptotic critical density (yellow density). The graph provides a suggestion that quantiles can be adjusted to have the Type I (false-positive) error rejection rate improved. Adjustment of the asymptotic critical value means finding a  $C_{\alpha^*}$  that satisfies

$$P(M_q > C_{\alpha^*}) = \alpha^* < \alpha \tag{28}$$

such that  $P(M_{n,\beta} > n^{-1/2}C_{\alpha^*}^* | H_0)$  is as close as possible to  $\alpha$ .

This can be done by solving the following equation:

$$P(M_q > C_{\alpha^*}) \approx P(M_{n,\beta} > n^{-1/2}C_{\alpha^*}^* | H_0). \tag{29}$$

The actual adjusted asymptotic critical values and applications will be presented in the simulation study.

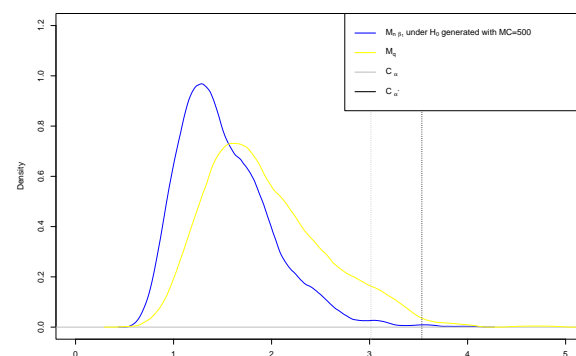


**Figure 2.**  $M_{n,\beta}$  under  $H_0$  kernel (Epanechnikov) density versus  $M_q$  kernel (Epanechnikov) density. Grey dotted line indicates  $\alpha = 0.01$  one-sided quantile, while grey dotted line provides adjusted quantile for  $\alpha = 0.01$ .

In the case where the operator  $\beta$  is unknown, the critical values can be adjusted also. Considering the case where the operator  $\beta$  in (1) is a multiplication by a function  $\beta(t), t \in [0, 1]$ , we define the following Algorithm 2.

**Algorithm 2** Adjusted quantiles procedure

1. Calculate  $\hat{\beta}(t)$  from the functional auto-regressive model defined in Equation (1)
2. Calculate  $\hat{Y}_k(t)$  by equation  $\hat{Y}_k(t) = X_{k+1}(t) - \hat{\beta}(t) X_k(t), k = 1, \dots, n$ . Afterwards, center the residuals  $\tilde{Y}_k(t) = \hat{Y}_k(t) - \frac{1}{n} \sum_{n=1}^k \hat{Y}_k(t), k = 1, \dots, n$ .
3. Draw randomly (with repetition) and with probability  $P(\tilde{Y}_n = Y_k^*) = \frac{1}{n}, k = 1, \dots, n$ , from  $\{\tilde{Y}_1, \tilde{Y}_2, \dots, \tilde{Y}_n\}$  to generate  $\{Y_1^*, Y_2^*, \dots, Y_n^*\}$ .
4. Generate new sample data  $\{X_1^*, X_2^*, \dots, X_n^*\}$  with the first moment by equation  $X_1^*(t) = X_1(t) = Y_1^*(t)$  and the following moments by equation  $X_k^*(t) = \hat{\beta}(t)X_{k-1}^* + Y_k^*, k = 1, \dots, n$ .
5. Use block bootstrap procedure, see Algorithm 1, with the length of the block  $l$  to draw from  $\{X_1^*, X_2^*, \dots, X_n^*\}$  new values  $\{X'_1, X'_2, \dots, X'_n\}$ . Then, calculate  $M'_{n,\hat{\beta}}$  from  $\{X'_1, X'_2, \dots, X'_k\}, k = 1, \dots, n$ , using Equation (12).
6. Repeat previous step as Monte Carlo simulations for MC times to construct  $\{M_{n,\hat{\beta}}^1, M_{n,\hat{\beta}}^2, \dots, M_{n,\hat{\beta}}^{MC}\}$ .
7. Adjust  $M_q$  quantile values with  $\{M_{n,\hat{\beta}}^1, M_{n,\hat{\beta}}^2, \dots, M_{n,\hat{\beta}}^{MC}\}$  to have Type I error minimized.

Algorithm 2 is built to solve the following equation:

$$P(M_{n,\beta} > C_\alpha) \approx P(M'_{n,\beta} > C_\alpha \mid X'_1, X'_2, \dots, X'_n) \approx P(M_q > C_\alpha). \tag{30}$$

A graphical interpretation of Algorithm 2 is presented in Figure 3. One can see that the initial  $M_{n,\hat{\beta}}$  density generated using the evaluated  $\hat{\beta}(t)$  is positioned with notable dispersion and a heavy tail to the right. Density improves with the following steps generating  $M^*_{n,\hat{\beta}}$ . Eventually, we have  $M'_{n,\hat{\beta}}$  density, which is close to  $M_q$ . An application of this algorithm will be presented in the case study.

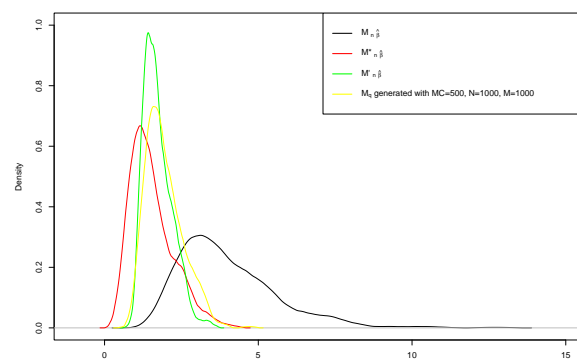


**Figure 3.** Algorithm 2 kernel (Epanechnikov) densities  $M_{n,\hat{\beta}}, M^*_{n,\hat{\beta}}$  and  $M'_{n,\hat{\beta}}$  versus  $M_q$  kernel (Epanechnikov) density.

**5. Simulation Study**

In this section, we consider the random functional sample  $X_i, i = 1, \dots, n$ , generated by the model

$$X_k(t) - \mu(t) = \beta(t)(X_{k-1}(t) - \mu(t)) + g(k/n, t) + Y_k(t), k = 1, \dots, n, \tag{31}$$

where the functions  $Y_k, k = 1, \dots, n$  are iid standard Wiener processes, and  $\beta = (\beta(t), t \in [0, 1])$  is a continuous function. We analyze test (22) in a Monte Carlo simulation study, distinguishing two cases:

- Case 1:  $g = 0$ , with the aim to test

$$H_0 : \mu = 0 \text{ versus } H_1 : \mu \neq 0.$$

- Case 2:  $\mu = 0$ , with the aim to test

$$H_0 : g = 0 \text{ versus } H_1 : g \neq 0.$$

In both cases, the following  $\beta$  functions are used:

$$\beta_1(t) = 0.7\sqrt{t}, \beta_2(t) = -0.7\sqrt{t}, \beta_3(t) = 0.7\sqrt{1-t}, \beta_4(t) = -0.7\sqrt{1-t}, t \in [0, 1]. \quad (32)$$

First we analyze the test statistic  $M_{n,\beta}$  for the model (31) under assumptions  $g = 0$  and  $\mu = 0$ . Figure 4 shows that coefficient  $b$  in  $\beta(t) = b\sqrt{t}, t \in [0, 1]$  has a minor effect on distribution of  $M_{n,\beta}$  if  $b < 0.7$ . If  $b$  exceeds 0.7 and approaches one, the  $M_{n,\beta}$  density is flattened and forced to the right. Moreover, Figure 5 indicates minor differences between the densities if different  $\beta_i(t), i = 1, \dots, 4$ , from Equation (32) are used. Therefore, in the following analysis, model (31) with  $\beta_1(t) = 0.7\sqrt{t}, t \in [0, 1]$  will be used. Simulations are performed with various  $n$  values: 100, 200, 500, 1000. These simulations are done for the null hypothesis with functions  $\mu(t) = 0$  and  $g(k/n, t) = 0$ ;  $\beta_1(t)$  is used in the following graphical analysis, and summary values are provided in a table for  $\beta_1(t), \beta_2(t), \beta_3(t)$ , and  $\beta_4(t)$ .

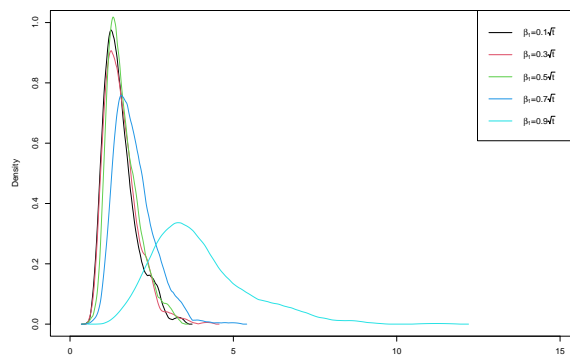


**Figure 4.**  $M_{n,\beta}$  kernel (Epanechnikov) densities under null hypothesis with  $\beta_1(t) = b\sqrt{t}(t)$ , where  $b = 0.1, b = 0.3, b = 0.5, b = 0.7, b = 0.9$ .

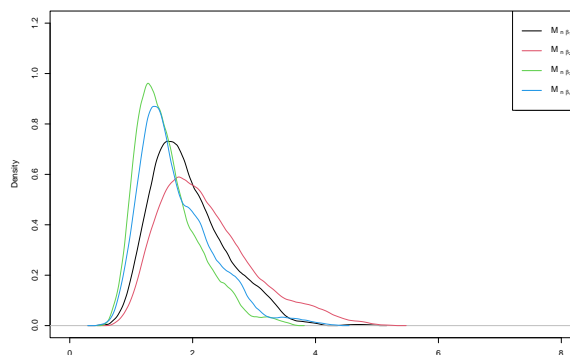


**Figure 5.**  $M_{n,\beta}$  kernel (Epanechnikov) densities under null hypothesis with  $\beta_1(t), \beta_1(t), \beta_3(t), \beta_4(t)$  and  $n = 1000$ .

### 5.1. False-Positive Rate

In this subsection, we are analyzing the false-positive or Type I error rate. We start with a comparison of the kernel density plots for  $M_{n,\beta}$  under  $H_0$  versus  $M_q$ . Figure 6a

shows that a higher  $n$  indicates that the density of the null hypothesis is moving towards the  $M_q$  density while  $n < 1000$ . This identifies a false-positive issue that can be seen from the graph—the test will conduct a significant number of false-positive errors if  $n \leq 1000$ .

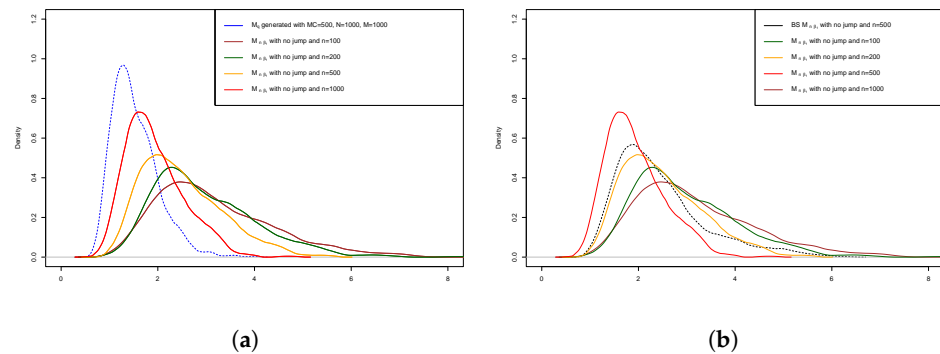


**Figure 6.**  $M_{n,\beta}$  under  $H_0$  densities with  $n = 100, n = 200, n = 100, n = 1000$  versus  $M_q$  (a) or block bootstrap  $M_{n,\beta}$  (b) densities. All densities estimated using Epanechnikov kernels.

Figure 7a implies that the Type I error rate decreases dramatically once  $n \geq 1000$ . We adjust asymptotic critical values by solving Equation (29) in order to minimize the Type I error rate. The adjusted asymptotic critical values corresponding to  $\beta_1(t), \beta_2(t), \beta_3(t), \beta_4(t)$  are given in Table 3. Indeed, the adjusted asymptotic critical values provide better results for false-positive cases: see Figure 7. This defines our upcoming steps: for further testing in simulations, adjusted one-sided asymptotic critical values will be used for  $n \geq 1000$ .

**Table 3.** Adjusted  $C_\alpha$  significance level  $\alpha$  values for  $\beta_1(t), \beta_2(t), \beta_3(t), \beta_4(t)$ .

|                 | $C_\alpha$ for $\beta_1$ | $C_\alpha$ for $\beta_2$ | $C_\alpha$ for $\beta_3$ | $C_\alpha$ for $\beta_4$ |
|-----------------|--------------------------|--------------------------|--------------------------|--------------------------|
| $\alpha = 0.01$ | 3.51                     | 3.51                     | 3.54                     | 3.51                     |
| $\alpha = 0.02$ | 3.41                     | 3.41                     | 3.42                     | 3.41                     |
| $\alpha = 0.05$ | 3.10                     | 3.15                     | 3.12                     | 3.1                      |

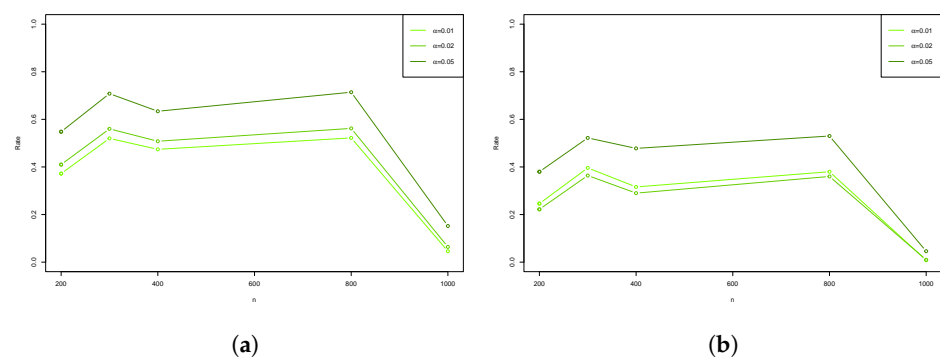


**Figure 7.** False-positive rate calculations conducted using different values for  $n, n \geq 200$  for adjusted (b) and non-adjusted (a) critical values. Colors stands for significance level  $\alpha$ ; hypothesis rejected using  $M_q$ .

If  $n < 1000$ , then we perform a block bootstrap by Algorithm 1. The great question is which block length is optimal. The question is answered by using generated bootstrap data with different block lengths  $l = \{2, 3, \dots, 10, 20, 50, 100, 200\}$ . The decision is reached by two criteria for errors (mean square error and mean absolute error): the most notable change in error by the elbow rule and the lowest error value. Eventually, this indicated that the best block length is equal to 4. After ascertaining all the parameters for Algorithm 1, we perform it MC = 500 times to calculate the sample of the test statistics  $Z = \{M_{n,\beta}^1, M_{n,\beta}^2, \dots, M_{n,\beta}^{500}\}$ . We calculate quantile values from  $Z$  and decide by the  $Z_{1-\alpha}$  value: we reject the null hypothesis with a significance level  $\alpha$  if  $M_{n,\beta}$  is higher than  $Z_{1-\alpha}$ .

The density plots in Figure 6b provide evidence that the block bootstrap is a good choice for the  $n = 100$  situation. The density plot for  $M_{n,\beta}$  generated with  $n = 100$  is observed in both Figure 6a,b in green color. If one compares this density with the  $M_q$  density graph in Figure 6a, it becomes evident that the densities corresponding to  $n = 100$  exhibit a sub-optimal degree of overlap with their associated  $M_q$  density values (dotted blue color). In Figure 6b, comparing the density in the relation between the  $n = 100$  density and the block bootstrap values (dotted black color), a noteworthy enhancement in the degree of overlap is observed. We ask how the block bootstrap procedure can help to avoid false-positive errors. Figure 8 implies that the procedure decreases the false positive rate by a notable amount. Figure 8a adds that the Type I error rate tested with block bootstrap critical values is stable when  $n \leq 100$ , and the false-positive rate stays under 0.4. Improved outcomes are evident for lower values of  $n$  if we apply the block bootstrap procedure.

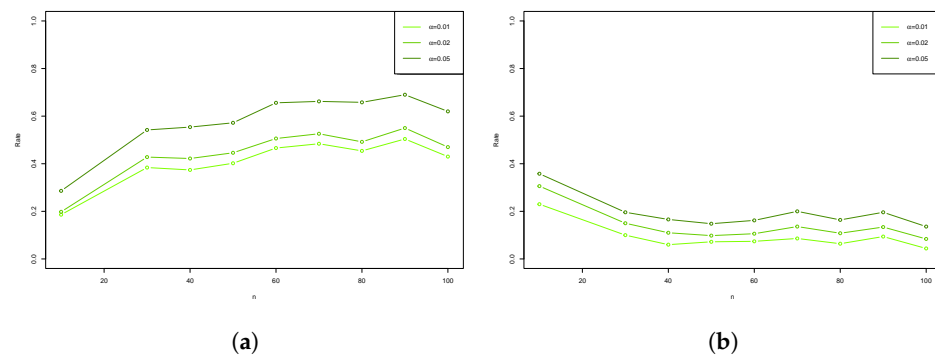


**Figure 8.** False-positive rate using  $M_q$  critical values (a) and  $M_{n,\beta}$  (b) block bootstrap for different significance levels  $\alpha$ .

To conclude the  $M_{n,\beta}$  under  $H_0$  graphical analysis, for cases with  $n \geq 1000$ , it is advised to use  $M_q$ , and for  $n < 100$ , use block bootstrap critical values of  $M_{n,\beta}$ . For  $n \in (100;1000)$ , we suggest using the block bootstrap procedure to generate quantile values or using adjusted asymptotic critical values.

5.2. Power Analysis

$Y_k(t)$  are iid standard Wiener processes. In this section, we have  $H_1 : g \neq 0$  or  $H_1 : \mu \neq 0$  depending on the case:

- Case 1

$$g = 0 \text{ and } \mu(a;t) = a\sqrt{t}. \tag{33}$$

- Case 2

$$\mu = 0 \text{ and } g_a(k/n;t) = a\sqrt{t} \mathbf{1}_{[k^*,n]}(k). \tag{34}$$

Simulation example graphs are provided in Figure 9 for deeper understanding. One can see that we might encounter issues as the grey curves (simulations with jumps) and the black curves (simulations with no jumps) overlap.

By testing different  $a$  values from the interval, we observe the test power, which is defined by the following probability:

$$P(M_{n,\beta} > C_\alpha | H_1) = \beta. \tag{35}$$

Power calculations in the following paragraph will be provided for two situations:  $n = 100$  and  $n = 1000$ . Moreover, calculations are done using block bootstrap critical values, see Algorithm 1, for  $n = 100$  and adjusted asymptotic critical values, see Algorithm 2, for  $n = 1000$ .

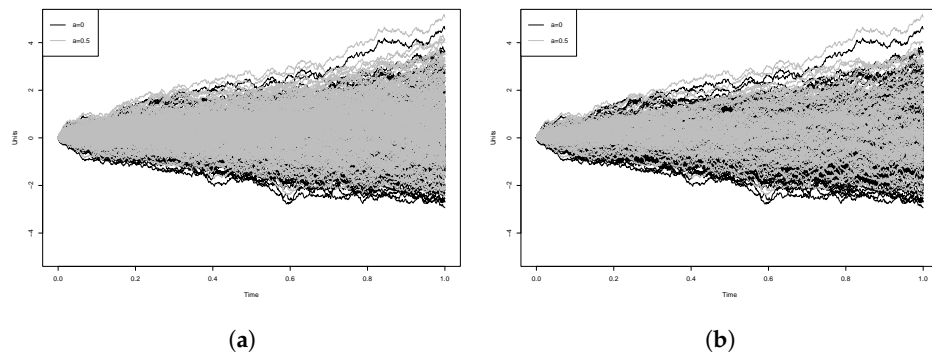


**Figure 9.** Simulations generated using Equation (31) with  $n = 200$  for both Case 1 and Case 2 jumps: (a) Case 1:  $\mu(a; t) = a\sqrt{t}$ ; (b) Case 2:  $g_a(k/n; t) = a\sqrt{t}\mathbf{1}_{[k^*, n]}(k)$ . Jump parameters for both cases are  $a = 0$  and  $a = 0.5$ .

Simulations commenced with the Case 1 scenario for different  $n$  values. Prior to delving into a comprehensive power analysis, we conduct an initial examination of the density plots. The examination is started with the simulated density plots in Figure 10, where the  $M_{n,\beta}$  density is simulated using jump parameter  $a = 0.5$ . Although the density graph in Figure 10a identifies that  $M_q$  quantiles can be used to test the change-point, the results are dissatisfying with  $n = 100$ . If the  $M_{n,\beta}$  block bootstrap is used, see Figure 10b, the results are better and the density plots have a higher degree of overlap than in the  $M_q$  case. The problem is solved when the jump parameter is higher,  $a = 1$ , and both  $M_q$  and the  $M_{n,\beta}$  block bootstrap can be used to identify the jump. Density plots as proof are provided in Figure 11a,b.

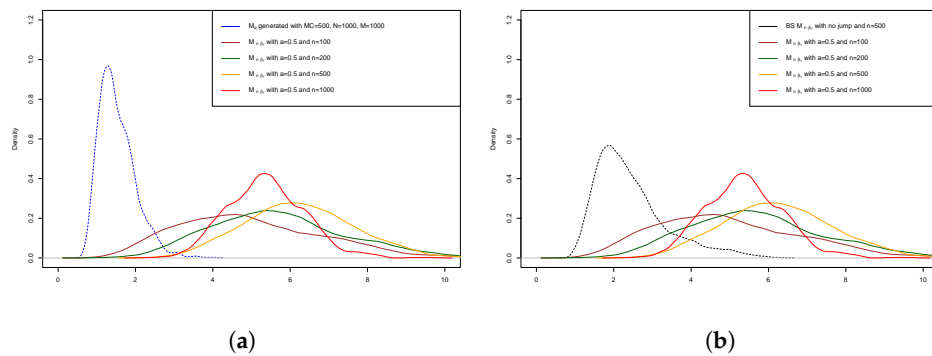


**Figure 10.** Case 1:  $H_1: a = 0.5$  densities with  $n = 100, n = 200, n = 500, n = 1000$  versus  $M_q$  (a) or block bootstrap  $M_{n,\beta}$  (b) densities. All densities estimated using Epanechnikov kernels.

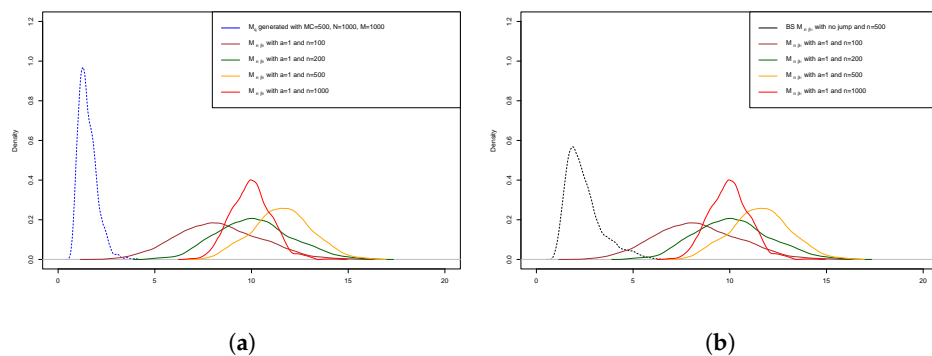


**Figure 11.** Case 1:  $H_1: a = 1$  densities with  $n = 100, n = 200, n = 500, n = 1000$  versus  $M_q$  (a) or block bootstrap  $M_{n,\beta}$  (b) densities. All densities estimated using Epanechnikov kernels.

Simulations were extended to the Case 2 scenario. The jump,  $k^*$ , is monitored after 25% of the sample size,  $n$ , is simulated. In other words,  $k^* = 0.25n$ . For example, if the simulation contains  $X_1(t), X_2(t), \dots, X_{100}(t)$ , then  $g_a(k/n, t) \neq 0$  in  $X_{25}(t), \dots, X_{100}(t)$ , and  $g_a(k/n, t) = 0$  elsewhere. We present density plots for the test statistics: see Figures 12 and 13. As before, two different jump parameter values are used for simulations:  $a = 0.5$  and  $a = 1$ . The density plots are compared between asymptotic critical values  $M_q$  and block bootstrap from  $M_{n,\beta}$  critical values. One can instantly identify that the density plots for the test statistics with both jump parameters ( $a = 0.5$  and  $a = 1$ ) in the Case 2 scenario tend to have increased dispersion in comparison to the Case 1 scenario. Wider dispersion and flat density plots identify a challenge to recognize the change-point for  $n \leq 500$  simulations using the critical values  $M_q$ : see Figure 12a. However, the density plots suggest that change-point identification can be improved if the block bootstrap values from  $M_{n,\beta}$  are used: see Figure 12b. If the jump value is increased to 1, the situation improves as the density plot tweaks to the right side: see Figure 13.

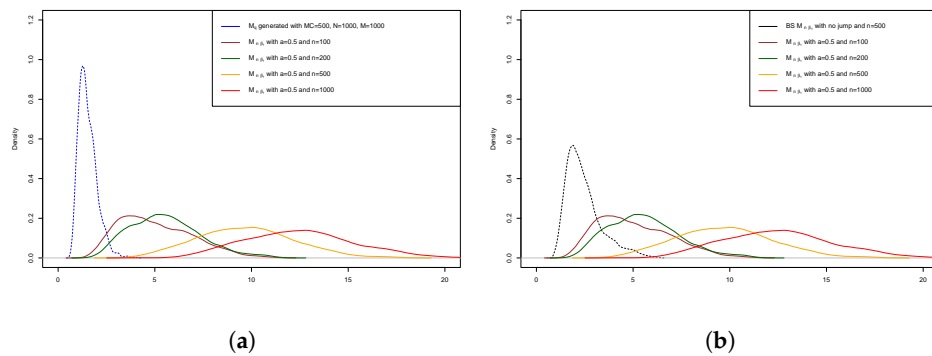


**Figure 12.** Case 2:  $H_1: a = 0.5$  densities with  $n = 100, n = 200, n = 500, n = 1000$  versus  $M_q$  (a) or block bootstrap  $M_{n,\beta}$  (b) densities. All densities estimated using Epanechnikov kernels.

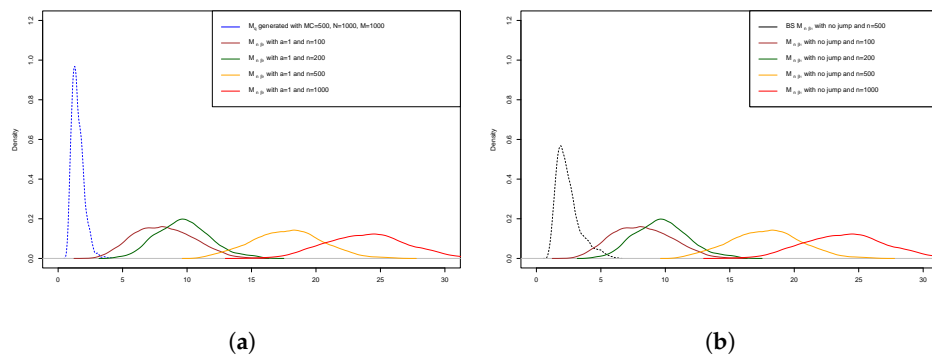


**Figure 13.** Case 2:  $H_1: a = 1$  densities with  $n = 100, n = 200, n = 500, n = 1000$  versus  $M_q$  (a) or block bootstrap  $M_{n,\beta}$  (b) densities. All densities estimated using Epanechnikov kernels.

A power analysis is started for the Case 1 scenario. Figure 14 provides power changes for different  $a$  values. As before,  $n = 100$  and  $n = 1000$  cases are provided and tested with the block bootstrap critical values from  $M_{n,\beta}$  and the adjusted asymptotic critical values from  $M_q$ , respectively. As one can see from Figure 14a, parameter  $a$  needs to reach 1.2 in order to gain power almost equal to 1 in the  $n = 100$  situation. As for  $n = 1000$ , the test can have a lower  $a$  value, 0.5, to gain power equal to 1. We continue with the power analysis for Case 2: see Figure 15. The results are similar to those for Case 1 for both  $n = 100$  and  $n = 1000$ . The main difference can be seen in Figure 15b, where the desired power value, 0.95, is reached faster when the jump parameter value  $a$  is equal to 0.3.

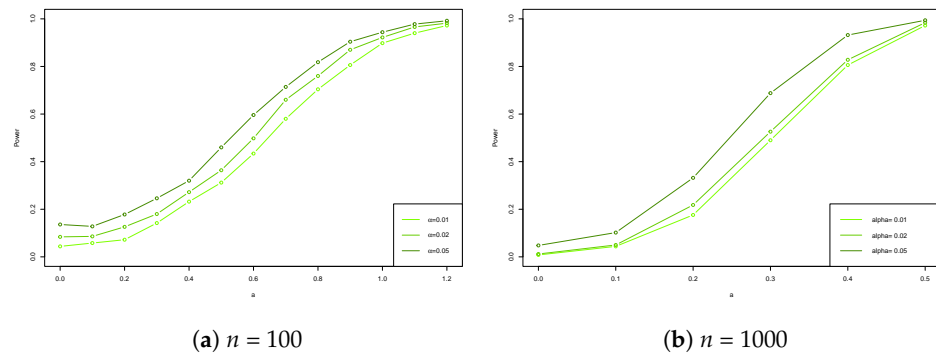


**Figure 14.** Case 1: Power change with  $H_1$  simulated using different jump parameters  $a$ . Power calculated using  $M_q$  (b) or block bootstrap  $M_{n,\beta}$  (a).

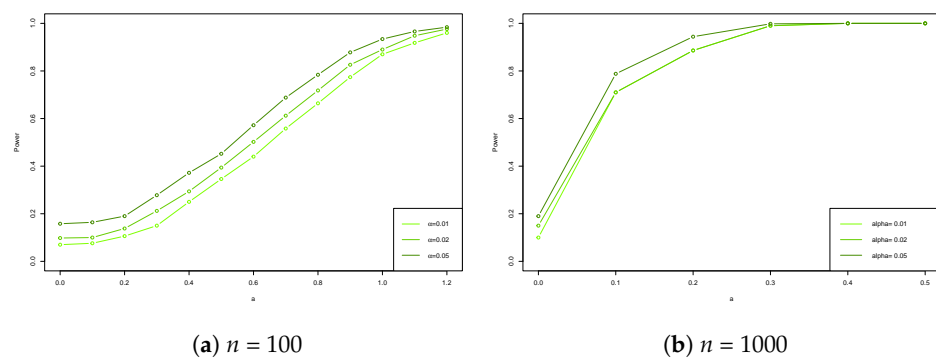


**Figure 15.** Case 2: Power change with  $H_1$  simulated using different jump parameters  $a$ . Power calculated using  $M_q$  (b) or block bootstrap  $M_{n,\beta}$  (a).

As we mentioned in the previous section,  $\beta(t)$  is usually unknown for  $M_{n,\beta}$ . The solution for such a problem requires  $\beta(t)$  to be replaced by  $\hat{\beta}(t)$ , and eventually  $M_{n,\hat{\beta}}$  needs to be used for the testing procedure. First, let us examine if we have significant fluctuations between the theoretical and evaluated  $\beta(t)$ . In Figure 16, one can find the theoretical  $\beta(t)$  provided in green color. Moreover,  $\hat{\beta}_{MC}(t)$  is provided for every Monte Carlo simulation in grey color, and the averaged value from all Monte Carlo simulations is provided in black color. The plot indicates that, on average, the difference between theoretical and evaluated coefficients is minor. However, some  $\hat{\beta}_{MC}(t)$  variations from the average can be noted. To conclude, in situations where  $\beta(t)$  is unknown, one needs to use  $\hat{\beta}(t)$  and calculate  $M_{n,\hat{\beta}}$  and compare it against  $M_q$  when  $n = 1000$ .

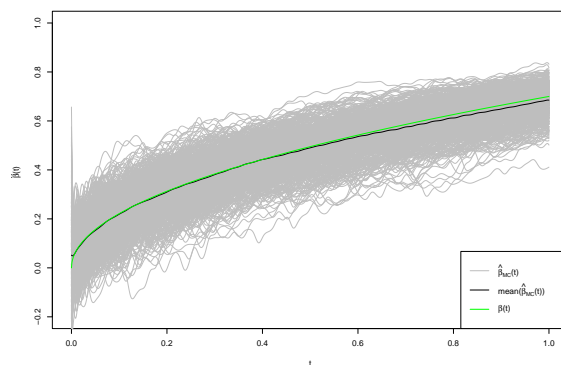


**Figure 16.**  $\hat{\beta}_{MC}(t)$  in grey color provides evaluated  $\beta(t)$  function from every simulation, while the average of all evaluated  $\hat{\beta}_{MC}(t)$  is in black color. Theoretical  $\beta(t)$  in black.

We might encounter a problem when data are  $n = 100$  as we need to calculate block bootstrap values from test statistics under the null hypothesis. In other words, for hypothesis testing the  $M_{n,\hat{\beta}}$  value needs to be compared against quantile values to compute  $M'_{n,\hat{\beta}}$ , which we define as  $M_{n,\hat{\beta}}$  under  $H_0$ : see Algorithm 2. For the  $M'_{n,\hat{\beta}}$  calculation, we use the block bootstrap procedure defined in Algorithm 1 with  $l = 4$ . Eventually,  $M_{n,\hat{\beta}}$  is compared with quantile values from  $M'_{n,\hat{\beta}}$  to either reject or accept  $H_0$  in any case scenario for  $n = 100$ .

Afterwards, we analyze how the test power is affected if we take  $\hat{\beta}(t)$  instead of  $\beta(t)$ . Figure 17 can answer this question. When the jump parameter value was elevated from 0 to 2, power, calculated with  $M_{n,\beta}$ , achieved a value equal to 1 with  $a = 1.2$ . For the power generated with  $M_{n,\hat{\beta}}$ , desired power level is gained with  $a = 1.7$ . To conclude, the test power faces minor drawbacks while moving from  $M_{n,\beta}$  to  $M_{n,\hat{\beta}}$ . However,  $M_{n,\hat{\beta}}$  manages to provide stable and desired power results.

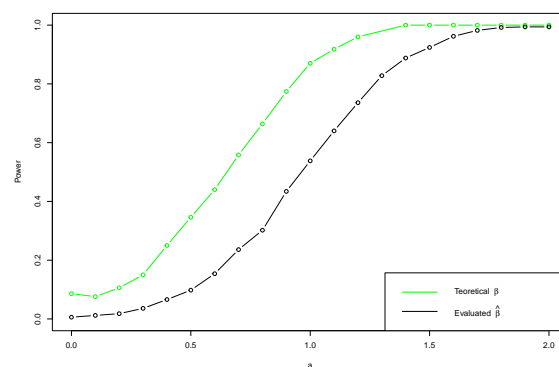


**Figure 17.** Simulations performed to understand how jump parameter affects power with  $\alpha = 0.01$ . Green color stands for power calculated with theoretical coefficient,  $M_{n,\beta}$ ; black color stands for power evaluated with FAR(1) coefficient  $M_{n,\hat{\beta}}$ . Jump parameter,  $a$ , advanced from 0 to 2.

Size-adjusted power graphs are provided for every scenario: see Figures 18 and 19. Size-adjusted power is the rate at which the null hypothesis is correctly rejected when the used critical value is stable with various  $n$  values. What we want to ensure here is that the test power is not affected by size distortions. Again, different  $a$  values,  $a = 0.1$ ,  $a = 0.5$  and  $a = 1$ , are used to understand how fast the desired power is reached using the predefined size of simulations when the jump is known and located proportionally to the sample size. For example,  $0.2n$  is 20% of the simulated sample data for the sample size  $n$ , and the jump is located at position  $k^* = 0.2n \times 0.25$ . The power is calculated empirically by using Monte Carlo simulations. Moreover, a significance level  $\alpha = 0.01$  is used for power calculation as it manages to provide the desired results.

Figure 18a identifies the Case 1, see Equation (34), scenario for  $n = 100$ . The graph implies that  $a = 0.5$  faces power instability until 20% of the sample and increases afterwards. The power reached a value of 0.4, with fluctuations during the increase. The results are better with  $a = 1$ : see Figure 18b. In the plot, fluctuations can be seen until 15% of the sample. Later increases are stable, without high fluctuations, and the plot eventually reaches power equal to 0.8 with 100% of the data. The size-adjusted power is calculated for the  $n = 1000$  situation: see the results in Figure 19. Figure 19a provides the size-adjusted power with a jump parameter equal to 0.1. The empirical power reaches a 0.76 power value after 60% of the sample size. The figure also indicates higher fluctuations than for the  $n = 100$  case. The results improve with  $a = 0.5$ , where the empirical power increases to 0.99 after reaching 20% of the sample size. Moreover, the rise of the curve faces only minor fluctuations, as can be seen in Figure 19b.

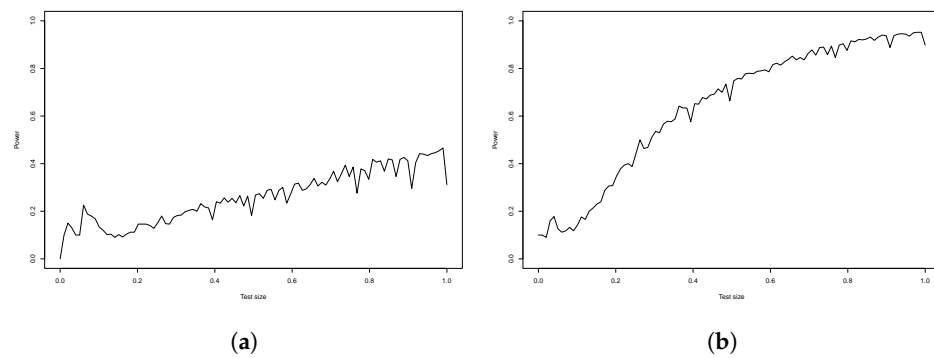


**Figure 18.** Case 1: Size-adjusted power calculated using using block bootstrap from  $M_{n,\beta}$  with  $\alpha = 0.01$ ,  $n = 100$ . Power with  $a = 0.5$  (a), and power with  $a = 1$  (b). Calculations are done for  $MC = 500$ .

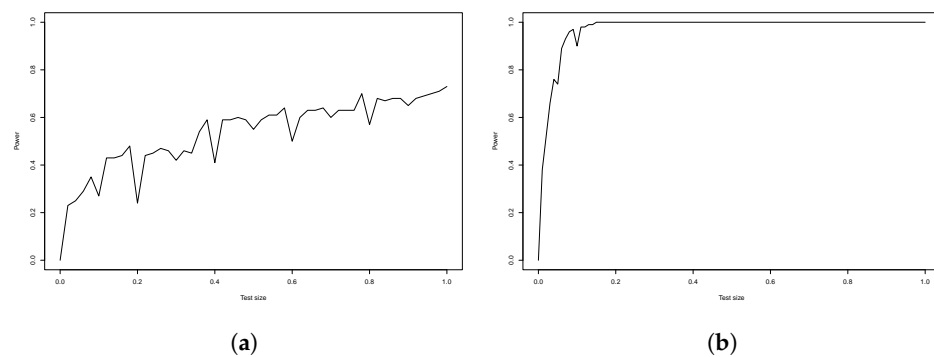


**Figure 19.** Case 1: Size-adjusted power calculated using using critical values from  $M_q$  with  $\alpha = 0.01$ ,  $n = 1000$ . Power with  $a = 0.1$  (a), and power with  $a = 0.5$  (b). Calculations are done for  $MC = 200$ .

We continue with the Case 2 scenario and the jump defined by Equation (34). Empirical power results are presented in Figures 20 and 21 for  $n = 100$  and  $n = 1000$ , respectively. As before, for  $n = 100$ , block bootstrap critical values from  $M_{n,\beta}$  are used for power calculation. The experimental findings indicate that the sample characterized by the jump parameter  $a = 0.5$  yields outcomes with statistical power achieving a value of 0.5 when the entire sample size is employed: see Figure 20b. In contrast, the sample featuring the jump parameter equal to 1 overcomes this power threshold, achieving a power value equal to 0.97 at the end of the sample: see Figure 20a. We resume with the  $n = 1000$  situation, where power was tested using adjusted asymptotic critical values from  $M_q$ . Figure 21a, simulated using  $a = 0.1$ , implies that the empirical power gain value of 0.6 using 40% of the sample size. However, the variation is notable in the graph. For  $a = 0.5$ , the results are significantly better: an empirical power of 0.98 is achieved with 25% of the sample size with minor variation.

We perform several additional analyses for Case 2. To begin with, a border analysis is conducted in order to understand overall test capabilities for the presented simulations at the borders of the sample with full period information. Simulations are run with jumps conducted at starting points  $(0.02n, 0.04n, \dots, 0.1n)$  and endpoints  $(0.9n, 0.92n, \dots, 0.98n)$ . In these simulations, we use  $n = 100$  for the block bootstrap critical values and  $n = 1000$  for the adjusted asymptotic critical values. The jump parameter,  $a$ , is equal to 1 for the  $n = 100$  situation and 0.5 for the  $n = 1000$  situation. For better visual understanding, simulated FAR(1) curves with defined  $n$  and  $a$  values are presented in Figure 22. A jump is conducted on the  $k^* = 0.02n$  observation. We can see that although the jump moves the curves upward, most of the grey curves (simulations with jump) overlap with the black curves (simulations with no jump). This means we might encounter issues if conducting an eye test. The jump test is conducted, and the results are presented in Figure 23. What needs to be emphasized is that the test is conducted with full information  $n$ . As one can notice, both situations

suggest that the test is not sensitive to the jump location. Figure 23a indicates that the desired power is reached from  $0.02n$  with no issues at the end of the interval. Figure 23b implies that power close to 1 is reached from  $0.02n$  to  $0.98n$  with slightly lower power if the jump is monitored at the end.

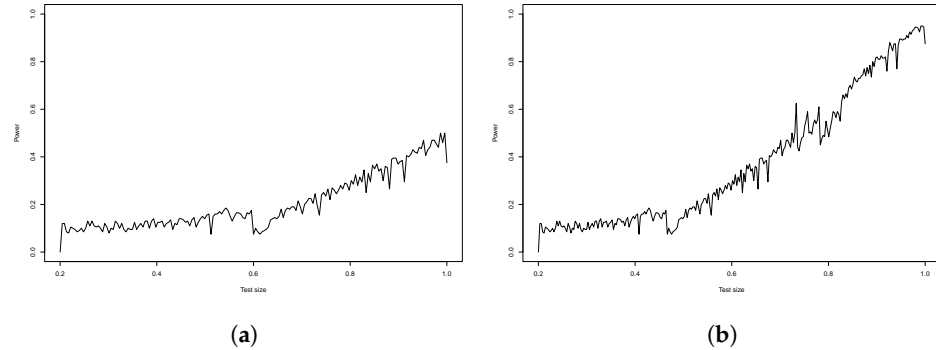


**Figure 20.** Case 2: Size-adjusted power calculated using block bootstrap from  $M_{n,\beta}$  with  $\alpha = 0.01$ ,  $n = 100$ . Power with  $a = 0.5$  (a), and power with  $a = 1$  (b). Calculations are done for  $MC = 500$ .

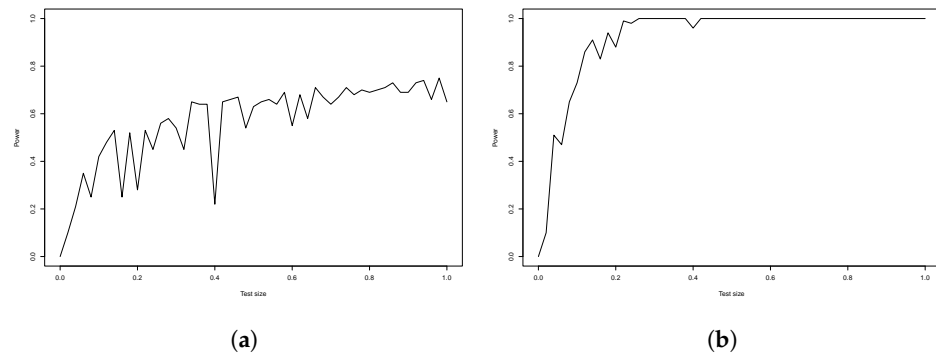


**Figure 21.** Case 2: Size-adjusted power calculated using using critical values from  $M_q$  with  $\alpha = 0.01$ ,  $n = 1000$ . Power with  $a = 0.1$  (a), and power with  $a = 0.5$  (b). Calculations are done for  $MC = 200$ .

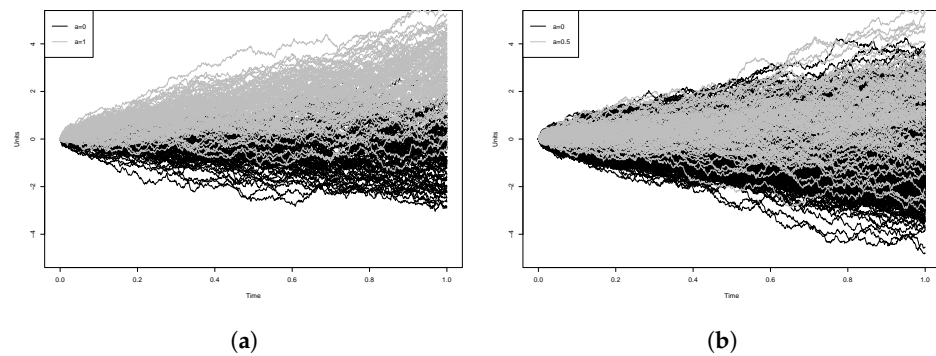


**Figure 22.** Simulation curves generated using Equation (31) with defined  $n$  and  $a$  values and jump on  $0.02n$ . (a)  $n = 100$  and  $a = 1$ ; (b)  $n = 1000$  and  $a = 0.5$ .

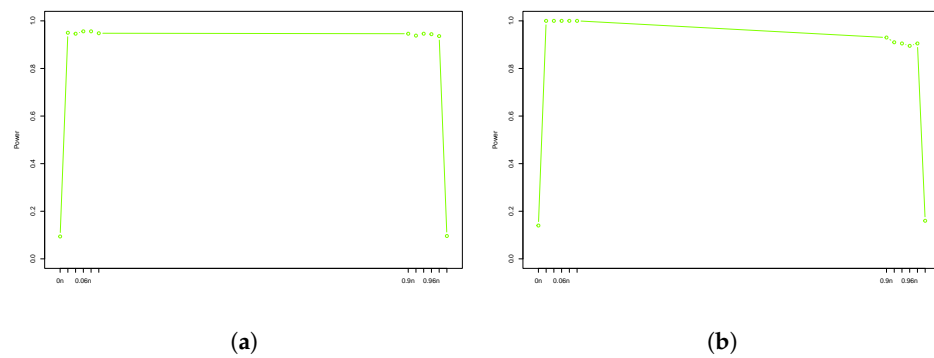


**Figure 23.** Simulations performed with jumps at the start and end of the interval in order to understand the location effect on power using significance level  $\alpha = 0.01$ . **(a)**  $n = 100$  and  $a = 1$ ; **(b)**  $n = 1000$  and  $a = 0.5$ .

We continued additional analyses with the offline method. The method retrospectively detects changes when all samples are received. In other words, in this situation, testing is conducted on the partial information  $k \leq n$ . For both situations,  $n = 100$  and  $n = 1000$ , simulations are fixed with the jump, Equation (34), at  $X_{25}(t)$  and  $X_{250}(t)$ , respectively. Graphical results are presented in Figure 24. For  $n = 100$ , one can notice that the first  $M_{n,\beta}$  values reach the red line, the  $C_\alpha$  value, at  $n = 30$ , while after  $n > 50$ , a significant number of curves reaches the same red line: see Figure 24a. For  $n = 1000$ , the results indicate a similar trend: the  $M_{n,\beta}$  values reach the  $C_\alpha$  value moments after the jump, at  $n > 250$ , and the number of curves over the red line gradually increases while  $n$  increases. This implies that for both  $n = 100$  and  $n = 1000$  in the Case 2 scenario, the test provides  $H_0$  rejections for some number of simulations moments after the jump. The number of curves over  $C_\alpha$  increases faster in relation to  $k$  with  $n = 1000$  than with  $n = 100$ .

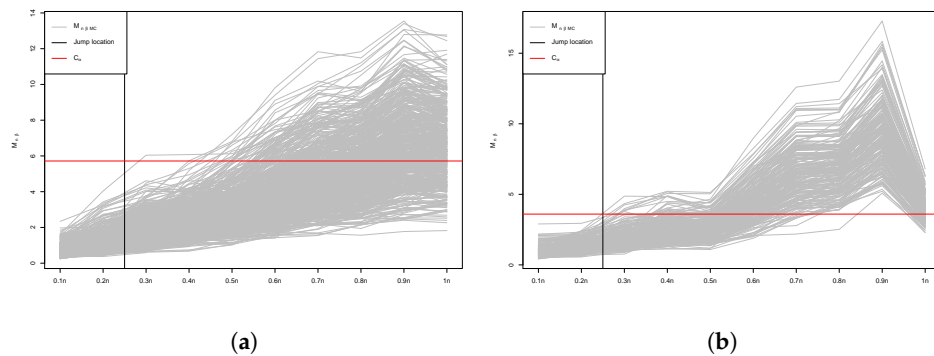


**Figure 24.** Total of 500 Monte Carlo simulations performed with jumps  $0.25n$  with significance level  $\alpha = 0.01$ . **(a)**  $n = 100$ ,  $a = 1$ , and **(b)**  $n = 1000$ ,  $a = 0.5$ .

To sum up, the test performed for situations where FAR(1), Equation (31), is generated using  $Y_k(t)$  was a standard normal Wiener process. Two types of scenarios, Case 1 and Case 2, helped to evaluate the test power. Multiple additional analyses were performed for Case 2. Moreover, two types of situations,  $n = 100$  and  $n = 1000$ , were used for calculating different test statistics. For the jumps defined in Equation (33) and Equation (34) for various  $a$  values, we indicated where the test performed well and where the test encountered issues. Overall, the test provided a positive outcome.

### 6. Case Study

In order to perform the test on real data, we employed a telecommunications data set. The data set was used by Birbilas and Račkauskas [20], who showed that the FAR(1) model is appropriate for prediction purposes. In this work, we continue the analysis of this data set by proposing a test for the detection of structural changes. The data are taken from a

telecommunications company that is operating in southern Europe. The data set contains voice and mobile data daily consumption for approximately 13k subscribers. The total monitored period was 31 months, starting December 2019. Consumption is aggregated by a summation procedure on a monthly basis. In order to move data to a functional space, consumption is converted to functions using b-spline functions with a basis equal to 10. Moreover, consumption is encapsulated to the interval  $t = [0,1]$  in order to have the same length during all months.

In order to have better understanding of how smoothing is performed, Figure 25a,b are provided as example cases for 20 randomly selected subscribers. As an example for better understanding of the data, Figure 26a has a whole year’s voice calls in minutes for 20 randomly selected subscribers. The same graph with mobile data consumption is provided in Figure 26b.

Indeed, the graphs identify that subscribers have various consumption patterns. One might notice that a number of jumps can be seen with an eye test despite which metric, voice consumption or mobile data consumption, is used. For further analysis, we will use voice consumption in minutes as a metric. Moreover, we do not find value in testing each of the 13k subscriber for jump patterns, and for further analyses, subscribers had to be clustered. Clustering is done by following these steps:

- A functional first-order auto-regression, FAR(1), is created for every subscriber. The total number of subscribers is  $z = 13,862$ .
- $\hat{\beta}_s^z(t)$  are taken from every FAR(1).
- $\hat{\beta}_s^z(t)$  are clustered into four groups using the Fisher-EM algorithm with k-means initialization. The best cluster is chosen by AIC criteria.

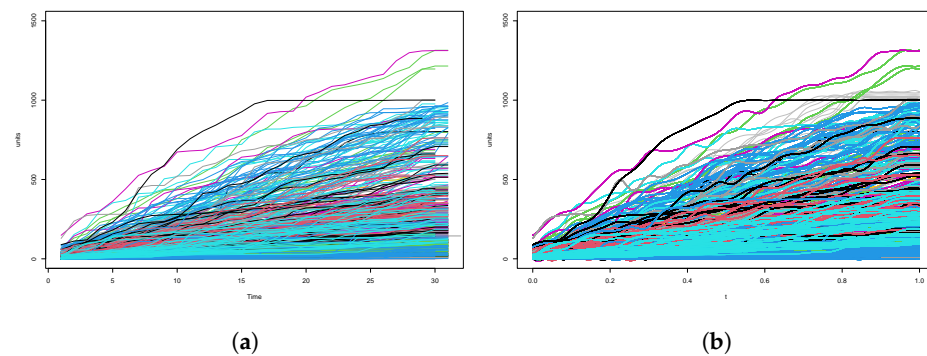


**Figure 25.** Raw (a) versus smoothed (b) data for 20 randomly selected subscribers. Colors represent different subscribers.

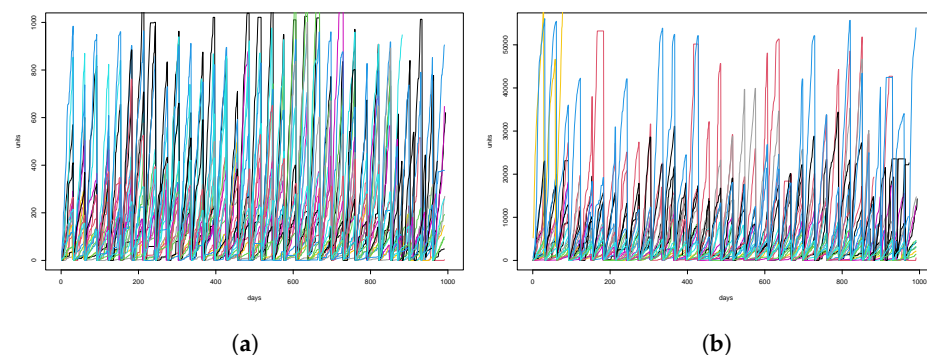


**Figure 26.** Voice call consumption in minutes (a) and mobile data consumption in MB (b) for 20 randomly selected subscribers. Colors represent different subscribers.

Additional filtering  $\hat{\beta}_s^z(t) \in (-1,1)$  is done in order to discard  $\hat{\beta}_s^z(t)$  from spurious auto-regressions. After filtering, we created four clusters using the Fisher-EM method. The results with the averaged  $\hat{\beta}_s(t)$  for clusters are provided in Figure 27.

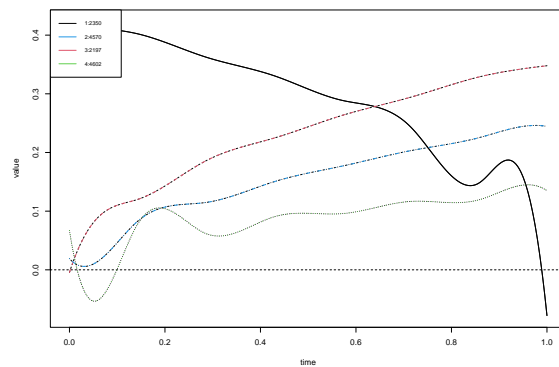


**Figure 27.** Clustering results with cluster centers. Legend provides cluster number with total subscribers within the cluster.

Analyses conducted on the clusters provided insights. In the first cluster, the majority of subscribers are old subscribers with stable consumption patterns. Most of them do not change their bundle plans, nor do they have their telecommunication services suspended. Figure 28a provides a better understanding of the average consumption within the first cluster. The second cluster contains subscribers who are frequent add-on users. We conclude that these subscribers tend to exhaust their bundle and purchase add-ons afterwards. This increases usage and creates average fluctuations: see Figure 28b. The third cluster contains more-or-less stable users. The only difference between this group and the first one is that subscribers in the third group tended to change their plans for the better. Telecommunications operators provided attractive offers during some months. This can be identified by increased average consumption in Figure 28c. In the last, fourth, cluster, we find that most of the subscribers are unstable users. For subscribers in this cluster, a stable activity period for several months is accompanied by no activity afterwards. Moreover, a significant number of subscribers within this cluster face service suspension due to insufficient funds during bundle renewal. Figure 28d provides averaged consumption for this cluster.

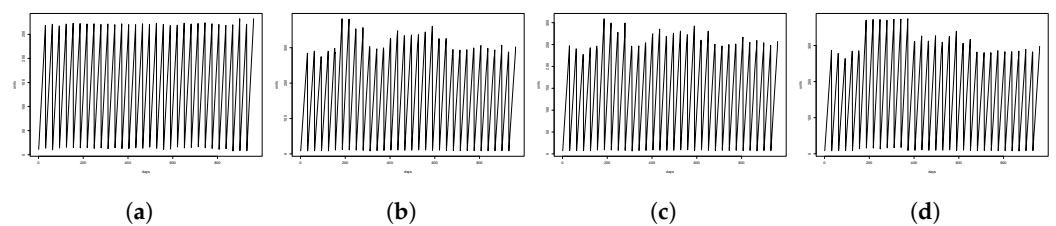


**Figure 28.** Averaged monthly consumption by cluster. (a) First cluster; (b) Second cluster; (c) Third cluster; (d) Fourth cluster.

The jump test is conducted on the created clusters. As one can see, only the first cluster (after excluding the last three months as outliers) is a candidate for no jump, while the second, third, and fourth clusters may even contain several jumps. A point-wise Box–Ljung test suggests ( $p$ -value  $> 0.05$ ) that all residuals of the model are not auto-correlated, as we cannot reject the null hypothesis of independence for model residuals. Moreover, the KPSS test suggests that residual increments are stationary, as we cannot reject the null hypothesis with confidence level  $\alpha = 0.01$ . Finally, visual interpretation and the Shapiro–Wilk test suggest that residual increments follow a normal distribution, as we cannot reject the null hypothesis of normality with the same confidence level. By completing the previous steps, we can state that our residual increments follow a Wiener (Brownian motion) process.

The jump test is performed for all four clusters. To have the Case 2 scenario have Equation (34) with  $\mu = 0$  and  $g(k/n; a; t) \neq 0$ , we centered our case study data. As  $n = 31$ , we used the blocked bootstrap critical values calculated using Algorithm 1 with the presented data. Although the strategy to identify jumps is the same between clusters,  $\hat{\beta}_t(s)$  differed

between the clusters: see Figure 27. This led to different block bootstrap quantile values from  $M_{n,\hat{\beta}}$  statistics and different  $H_0$  rejection critical values. Moreover, for the real-data situation, we used an estimated FAR(1) parameter:  $\hat{\beta}_t(s)$ . Eventually, the test implied no jump in the first cluster, see Figure 29a, and jumps in the other clusters, see Figure 29b–d, with the significance levels  $\alpha = 0.01$ . The results did match the eye test—the first cluster contains few outliers at the end of the interval and no jump, while the other clusters contain one or several jumps.

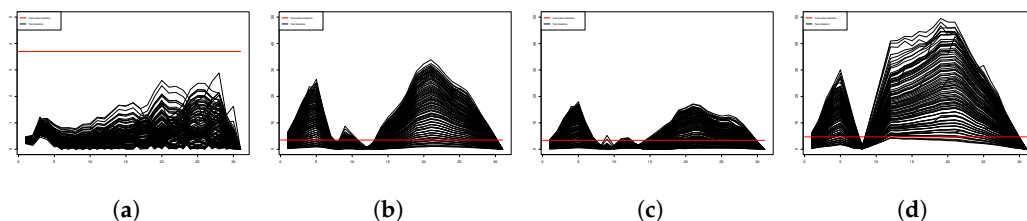


**Figure 29.** Test statistics versus calculated statistics by cluster. (a) First cluster; (b) Second cluster; (c) Third cluster; (d) Fourth cluster.

To conclude, eye-test assumptions were confirmed by the jump test. The first cluster had no proof to reject  $H_0$  with the defined significance level. All the other clusters had  $H_0$  rejected. The jump test performed well for the case study data.

**Author Contributions:** Conceptualization, A.R. and A.B.; methodology, A.R. and A.B.; software, A.R. and A.B.; validation, A.R. and A.B.; formal analysis, A.R. and A.B.; investigation, A.R. and A.B.; data curation, A.R. and A.B.; writing—original draft preparation, A.R. and A.B.; visualization, A.R. and A.B.; supervision, A.R. and A.B. All authors have read and agreed to the published version of the manuscript.

**Funding:** This research received no external funding.

**Data Availability Statement:** The data presented in this study are available on request from the corresponding author.

**Conflicts of Interest:** The authors declare no conflicts of interest.

## References

1. Aue, A.; Horváth, L. Structural breaks in time series. *J. Time Ser. Anal.* **2013**, *34*, 1–16. [[CrossRef](#)]
2. Zhu, X.; Li, Y.; Liang, C.; Chen, J.; Wu, D. Copula based change-point Detection for Financial Contagion in Chinese Banking. *Procedia Comput. Sci.* **2013**, *17*, 619–626. [[CrossRef](#)]
3. Garcia, R.; Perron, P. An Analysis of the Real Interest Rate Under Regime Shifts. *Rev. Econ. Stat.* **1996**, *78*, 111–125. [[CrossRef](#)]
4. Beaulieu, C.; Chen, J.; Sarmiento, J.L. Change-point analysis as a tool to detect abrupt climate variations. *Philos. Trans. R. Soc.* **2012**, *370*, 1228–1249. [[CrossRef](#)]
5. Ramsay, J.O. When the data are functions. *Psychometrika* **1982**, *47*, 379–396. [[CrossRef](#)]
6. Kokoszka, P.; Reimherr, M. *Introduction to Functional Data Analysis*; Chapman & Hall/CRC Texts in Statistical Science; Chapman and Hall/CRC: Boca Raton, FL, USA, 2018.
7. Ramsay, J.O.; Hooker, G.; Graves, S. *Functional Data Analysis*; Springer Series in Statistics; Springer: Berlin/Heidelberg, Germany, 2009.
8. Ramsay, J.O.; Hooker, G.; Graves, S. *Functional Data Analysis with R and MATLAB*; Springer: Berlin/Heidelberg, Germany, 2009.
9. Aneiros, G.; Cao, R.; Vilar-Fernandez, J.M.; Munoz-San-Roque, A. Functional Prediction for the Residual Demand in Electricity Spot Markets. *Recent Adv. Funct. Data Anal. Relat. Top.* **2011**, *1*, 4201–4208. [[CrossRef](#)]
10. Alaya, M.; Ternynck, C.; Dabo-Niang, S.; Chebana, F.; Ouardas, T. Change-point detection of flood events using a functional data framework. *Adv. Water Resour.* **2020**, *137*. [[CrossRef](#)]
11. Koerner, F.; Anderson, J.; Fincham, J.; Kassa, R. Change-point detection of cognitive states across multiple trials in functional neuroimaging. *Stat. Med.* **2016**, *36*, 618–642. [[CrossRef](#)]
12. Berkes, I.; Gabrys, R.; Horváth, L.; Kokoszka, P. Detecting changes in the mean of functional observations. *J. R. Stat. Soc. Ser. (Stat. Methodol.)* **2009**, *71*, 927–946. [[CrossRef](#)]
13. Aue, A.; Gabrys, R.; Horváth, L.; Kokoszka, P. Estimation of a change-point in the mean function of functional data. *J. Multivar. Anal.* **2009**, *100*, 2254–2269. [[CrossRef](#)]
14. Horváth, L.; Kokoszka, P.; Rice, G. Testing stationarity of functional data. *J. Econom.* **2014**, *179*, 66–82. [[CrossRef](#)]

15. Horváth, L.; Reeder, R. Detecting changes in functional linear models. *J. Multivar. Anal.* **2012**, *111*, 310–334. [[CrossRef](#)]
16. Aue, A.; van Delft, A. Testing for stationarity of functional time series in the frequency domain. *Ann. Stat.* **2020**, *48*, 2505–2547. [[CrossRef](#)]
17. Danielius, T.; Račkauskas, A. p-Variation of CUSUM process and testing change in the mean. *Commun. Stat. Simul. Comput.* **2020**, *52*, 1–13. [[CrossRef](#)]
18. Aspirot, L.; Bertin, K.; Perera, G. Asymptotic normality of the Nadaraya–Watson estimator for nonstationary functional data and applications to telecommunications. *J. Nonparametric Stat.* **2009**, *21*, 535–551. [[CrossRef](#)]
19. Yu, Y.; Lambert, D. Fitting Trees to Functional Data, with an Application to Time-of-Day Patterns. *J. Comput. Graph. Stat.* **1999**, *8*, 749–762. [[CrossRef](#)]
20. Birbilas, A.; Račkauskas, A. Functional modelling of telecommunications data. *Math. Model. Anal.* **2022**, *27*, 117–133. [[CrossRef](#)]
21. Shields, A.; Doody, P.; Scully, T. Application of multiple change-point detection methods to large urban telecommunication networks. In Proceedings of the 28th Irish Signals and Systems Conference (ISSC), Killarney, Ireland, 20–21 June 2017; pp. 1–6. [[CrossRef](#)]
22. Loreh, J. *Changepoint Analysis in the Wireless Telecommunications Industry*; Colorado School of Mines, ProQuest Dissertations Publishing: Ann Arbor, MI, USA, 2013. Available online: <https://hdl.handle.net/11124/80121> (accessed on 1 February 2023).
23. Aleksiejunas, R.; Garuolis, D. Usage of Published Network Traffic Datasets for Anomaly and Change Point Detection. *Wireless Pers. Commun.* **2023**, *133*, 1281–1303. [[CrossRef](#)]
24. Račkauskas, A.; Suquet, C. On limit theorems for Banach-space-valued linear processes. *Lith. Math. J.* **2010**, *50*, 71–87. [[CrossRef](#)]
25. Billingsley, P. *Convergence of Probability Measures*; John Wiley & Sons: Hoboken, NJ, USA, 1999.
26. Kuelbs, J. The invariance principle for Banach space valued random variables. *J. Multivar. Anal.* **1973**, *3*, 161–172. [[CrossRef](#)]
27. Härdle, W.; Horowitz, J.; Kreiss, J.P. Bootstrap Methods for Time Series. *Int. Stat. Rev.* **2003**, *71*, 435–459. [[CrossRef](#)]
28. Kunsch, H.R. The jackknife and the bootstrap for general stationary observations. *Ann. Stat.* **1993**, *17*, 1217–1261. [[CrossRef](#)]
29. Liu, R.Y.; Singh, K. Moving blocks jackknife and bootstrap capture weak dependence. *Explor. Limits Bootstrap* **1992**, *1*, 225–248.
30. Nyarige, E.U. The Bootstrap for the Functional Autoregressive Model FAR(1). Ph.D. Thesis, Kaiserslautern Technical University, Kaiserslautern, Germany, 2016. Available online: <https://d-nb.info/1106250273/34> (accessed on 1 April 2023).
31. Haynes, W. Bonferroni Correction. *Encycl. Syst. Biol.* **2013**, *1*, 154. [[CrossRef](#)]
32. Sedgwick, P. Multiple significance tests: The Bonferroni correction. *BMJ* **2012**, *344*, 509. [[CrossRef](#)]

**Disclaimer/Publisher’s Note:** The statements, opinions and data contained in all publications are solely those of the individual author(s) and contributor(s) and not of MDPI and/or the editor(s). MDPI and/or the editor(s) disclaim responsibility for any injury to people or property resulting from any ideas, methods, instructions or products referred to in the content.